Environmental Science & Technology

pubs.acs.org/est

Article

Mercury and Sulfur Redox Cycling Affect Methylmercury Levels in Rice Paddy Soils across a Contamination Gradient

Jiang Liu, Ji Chen, Alexandre J. Poulain, Qiang Pu, Zhengdong Hao, Bo Meng,* and Xinbin Feng

Cite This: *Environ. Sci. Technol.* 2023, 57, 8149−8160

Read Online

ACCESS | Metrics & More | Article Recommendations | Supporting Information

ABSTRACT: Methylmercury (MeHg) contamination in rice via paddy soils is an emerging global environmental issue. An understanding of mercury (Hg) transformation processes in paddy soils is urgently needed in order to control Hg contamination of human food and related health impacts. Sulfur (S)-regulated Hg transformation is one important process that controls Hg cycling in agricultural fields. In this study, Hg transformation processes, such as methylation, demethylation, oxidation, and reduction, and their responses to S input (sulfate and thiosulfate) in paddy soils with a Hg contamination gradient were elucidated simultaneously using a multi-compound-specific isotope labeling technique ($^{200}Hg^{II}$, $Me^{198}Hg$, and $^{202}Hg^{0}$). In addition to Hg^{II} methylation and MeHg demethylation, this study revealed that microbially mediated reduction of Hg^{II}, methylation of Hg^{0}, and oxidative demethylation−reduction of MeHg occurred under dark conditions; these processes served to transform Hg between different species (Hg^{0}, Hg^{II}, and MeHg) in flooded paddy soils. Rapid redox recycling of Hg species contributed to Hg speciation resetting, which promoted the transformation between Hg^{0} and MeHg by generating bioavailable Hg^{II} for fuel methylation. Sulfur input also likely affected the microbial community structure and functional profile of Hg^{II} methylators and, therefore, influenced Hg^{II} methylation. The findings of this study contribute to our understanding of Hg transformation processes in paddy soils and provide much-needed knowledge for assessing Hg risks in hydrological fluctuation-regulated ecosystems.

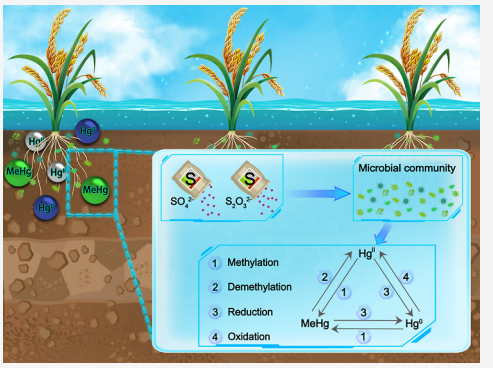

KEYWORDS: *Hg transformation, sulfur amended, paddy soil, multi-compound-specific isotope labeling*

1. INTRODUCTION

Over the last few decades, mercury (Hg) cycling in hydrological fluctuation-regulated ecosystems (e.g., wetlands, hydroelectric reservoirs, and paddy soils) has gained extensive attention. This is because, in these ecosystems, inorganic Hg is more readily transformed into toxic and bioaccumulative methylmercury (MeHg), as compared to other ecosystem types.[1−7] As a type of wetland, rice paddy fields play an important role in human MeHg exposure, especially in Hg-contaminated areas.[8,9] This is because rice (*Oryza sativa* L.) bioaccumulates MeHg[10,11] and paddy soil is a unique source of MeHg in rice.[12−16] Since rice is a staple food for a large proportion of the population worldwide, MeHg-contaminated rice and the resulting MeHg exposure risks are recognized as a global issue.[17−19] Therefore, a comprehensive understanding of the biogeochemical cycling of Hg in paddy soils is urgently required.

The transformation of Hg species in rice paddy ecosystems plays a vital role in Hg bioaccumulation and associated human exposure risks. Of particular importance are Hg methylation, demethylation, reduction, and oxidation; most of these processes are predominantly mediated by microorganisms.[20] Existing studies have mostly focused on methylation and demethylation,[3,4,21,22] with little attention paid to the reduction and oxidation processes. Thus, at present, we have an incomplete picture of Hg cycling in rice paddy soils. How redox processes affect (de)methylation remains unclear. Furthermore, most existing studies have only investigated bulk concentration changes in Hg species in rice paddies, with little study of interconversion processes.[3,4,23,24] Again, this has limited our understanding of net MeHg production mechanisms. Several studies have spiked stable Hg isotope tracers into rice paddy systems to simultaneously trace different transformation processes, including methylation and demethylation,[3,4,22,25] partitioning and redistribution,[26] and rice plant uptake and translocation.[15,27,28] However, only Hg^{II} or MeHg tracers have been applied to date, and only isotopic signals of THg or MeHg were measured in these studies. As a result, the redox processes of Hg in rice paddy systems have not yet been precisely traced.

Received: April 10, 2023
Revised: May 5, 2023
Accepted: May 5, 2023
Published: May 17, 2023

Wetlands are vital to the coupled biogeochemical cycles of Hg and sulfur (S).[29] On the one hand, sulfate reduction to sulfide and sulfide re-oxidation control the speciation and bioavailability of Hg by forming Hg−S compounds.[29−31] Recent studies have confirmed that the bioavailability of Hg substrates in methylation is determined not only by the formation of dissolved Hg−S complexes [e.g., $Hg(SH)_2$, HgS_2H^-, HgS_2^{2-}, $Hg(SR)_2$, etc.][30,31] but also by the intracellular dissolution of HgS nanoparticles.[25,32−34] On the other hand, sulfate reduction mediated by microorganisms is an important pathway for Hg methylation in natural environments.[35] For the reasons above, S input, especially atmospheric S deposition, is recognized as a major controlling factor in the production of MeHg.[36−39] More recently, however, a shift from atmospheric deposition to agricultural addition was reported as a new influencer of S cycling, and the role of S fertilizers in Hg transformation in agricultural fields was highlighted.[40] In the United States, agricultural S application exceeded ∼3.3 Tg yr^{-1} in 2017 (equal to ∼39.8 kg S ha^{-1} yr^{-1}),[40] and this number is projected to increase due to the decline in atmospheric S deposition and resulting S deficiencies in agricultural soils.[41] In China, where SO_2 emissions have declined from 21.85 Tg S yr^{-1} in 2011 to 3.18 Tg S yr^{-1} in 2021,[42] increasing application of S fertilizers has been reported.[43] Together, these estimates suggest that agricultural S additions are on par with atmospheric S deposition.[40] Therefore, S-regulated Hg transformation in agricultural fields (e.g., paddy soils) requires more attention. To date, limited studies have examined S input-influenced Hg transformation in paddy soils, with both promotion and inhibition of Hg^{II} methylation reported.[44−47] Most of these studies were based on bulk Hg concentration measurements, with little investigation of the precise transformation processes of Hg. Moreover, S species with different valent states determine the redox cycling of S and, thus, influence Hg transformation.[29] Accordingly, the role of different S species in Hg transformation is expected to be differential.

Here, a multi-compound-specific isotope labeling technique was employed together with sulfate and thiosulfate amendments of paddy soil to track Hg methylation, demethylation, oxidation, and reduction, simultaneously. Hg isotope labeling ($^{200}Hg^{II}$, $Me^{198}Hg$, and $^{202}Hg^0$) and geochemical and microbial approaches were combined to reveal Hg transformation in paddy soils and the underlying biogeochemical mechanisms. In addition to MeHg, isotopic signals of Hg^0 were determined, providing a more integrated understanding of Hg methylation, demethylation, oxidation, and reduction in paddy soils. In particular, the Hg transformation mechanisms were addressed in this study, especially S-regulated Hg transformation in paddy soils. Knowledge gained from this study can contribute to an improved understanding of Hg biogeochemistry in hydrological fluctuation-regulated ecosystems.

2. MATERIALS AND METHODS

2.1. Sample Collection. Rice paddy soil (surface soil, 1−5 cm) and overlying water samples were collected from three paddy fields. The first was an abandoned Hg mining site (SK, E 109°12′38″, N 27°31′2″) and the second was an artisanal Hg smelting site (GX, E 109°11′30″, N 27°33′50″) in the Wanshan Hg mining area (Wanshan District, Tongren City, Guizhou Province, China). The third was a control site in a rural area close to Guiyang City in Guizhou Province (HX, E 106°31′28″, N 26°25′20″). More detailed descriptions of the sampling sites are provided in Text S1 in the Supporting Information.

2.2. Preparation of Hg Isotope Tracers. Multi-compound-specific Hg isotope tracers, including the inorganic divalent Hg tracer ($^{200}Hg^{II}$), methyl-Hg tracer ($Me^{198}Hg$), and elemental Hg tracer ($^{202}Hg^0$), were used to trace Hg methylation (i.e., from $^{200}Hg^{II}$ to $Me^{200}Hg$ and from $^{202}Hg^0$ to $Me^{202}Hg$), MeHg demethylation (i.e., $Me^{198}Hg$ losses), Hg reduction (i.e., from $^{200}Hg^{II}$ to $^{200}Hg^0$ and from $Me^{198}Hg$ to $^{198}Hg^0$), and Hg oxidation/immobilization (i.e., $^{202}Hg^0$ losses). The preparation details are presented in Text S2.

2.3. Incubation Experiment Design. Serum bottles (100 mL, borosilicate glass bottle) were used for the anaerobic incubation experiment in an oxygen-free glovebox (PLAS-LABS, USA). Paddy soil and overlying water were mixed in the glovebox to prepare incubation slurries from each site, as described by Wu et al.[22] and Liu et al.[25] (see Text S3). Each homogenized slurry (30 mL) was weighed into a serum bottle. The moisture content of the prepared slurries (SK, GX and HX) was around 75% (Text S3). Four treatments, including sulfate (Na_2SO_4) and thiosulfate ($Na_2S_2O_3$) addition treatments as well as an autoclaved treatment (121 °C for 30 min) and a control treatment, were prepared. The same amount of S (equivalent to 2 mg of S) was added to each of the incubation bottles for the two S treatments. The dosage of exogenous S was similar to the total S content of paddy soils from Wanshan (∼200 mg kg^{-1}, ref 48). Isotope-enriched $^{200}Hg^{II}$, $Me^{198}Hg$, and $^{202}Hg^0$ tracers were spiked into all incubation bottles; the spiking dosage of Hg tracers depended on the ambient Hg concentration at each site (Table S1). Then, the incubation bottles were immediately sealed and gently shaken to mix the tracers and slurries. They were then covered with aluminum foil. The total period of incubation was 48 h (at 25 °C in the glovebox), and three random bottles (triplicates for each site and each treatment) were destructively sampled at 0 h, 12, 24, and 48 h. However, due to the periods of incubation, bottle preparation, and subsampling, the actual time series for purgeable Hg^0 was 2, 14, 26, and 50 h, and for MeHg, it was 4, 18, 28, and 52 h (see Text S4.1). After incubation, the isotope-enriched Hg^0 species ($^{198}Hg^0$, $^{200}Hg^0$, and $^{202}Hg^0$), MeHg species ($Me^{198}Hg$, $Me^{200}Hg$, and $Me^{202}Hg$), redox couples (HS^-/SO_4^{2-}, NO_3^-/NH_4^+, and Fe^{2+}/Fe^{3+}), and the concentration and optical properties (i.e., UV−vis absorption and fluorescence spectra) of water extracted soil dissolved organic matter (DOM) were determined. Genomic DNA was extracted for the quantification of functional genes that encode Hg and S transformations (*hgc*A, *mer*A, *mer*B, *dsr*B, and *sox*B). Hg-methylating microbial communities were identified by *hgcA* gene amplicon sequencing and metagenomic analysis, and the sequence data were deposited in the National Centre for Biotechnology Information (NCBI, https://www.ncbi.nlm.nih.gov/), with accession numbers PRJNA950218 and PRJNA950935, respectively. More details on the subsampling and measurements are provided in Text S4. The primers used for quantitative PCR are listed in Table S2.

2.4. Data Analysis. Ambient Hg refers to the Hg that is naturally present in the soil, and isotope-enriched Hg (^{198}Hg, ^{200}Hg, and ^{202}Hg) refers to Hg from the spiked tracers.[49,50] Mass-bias corrected signals of ambient Hg and Hg tracers were calculated using a simplified approach due to the negligible differences as compared to the matrix-based signal deconvolution approach[51] (Figure S1). Details related to the signal calculation and comparison methods can be found in Text S5.

https://doi.org/10.1021/acs.est.3c02676
Environ. Sci. Technol. 2023, 57, 8149−8160

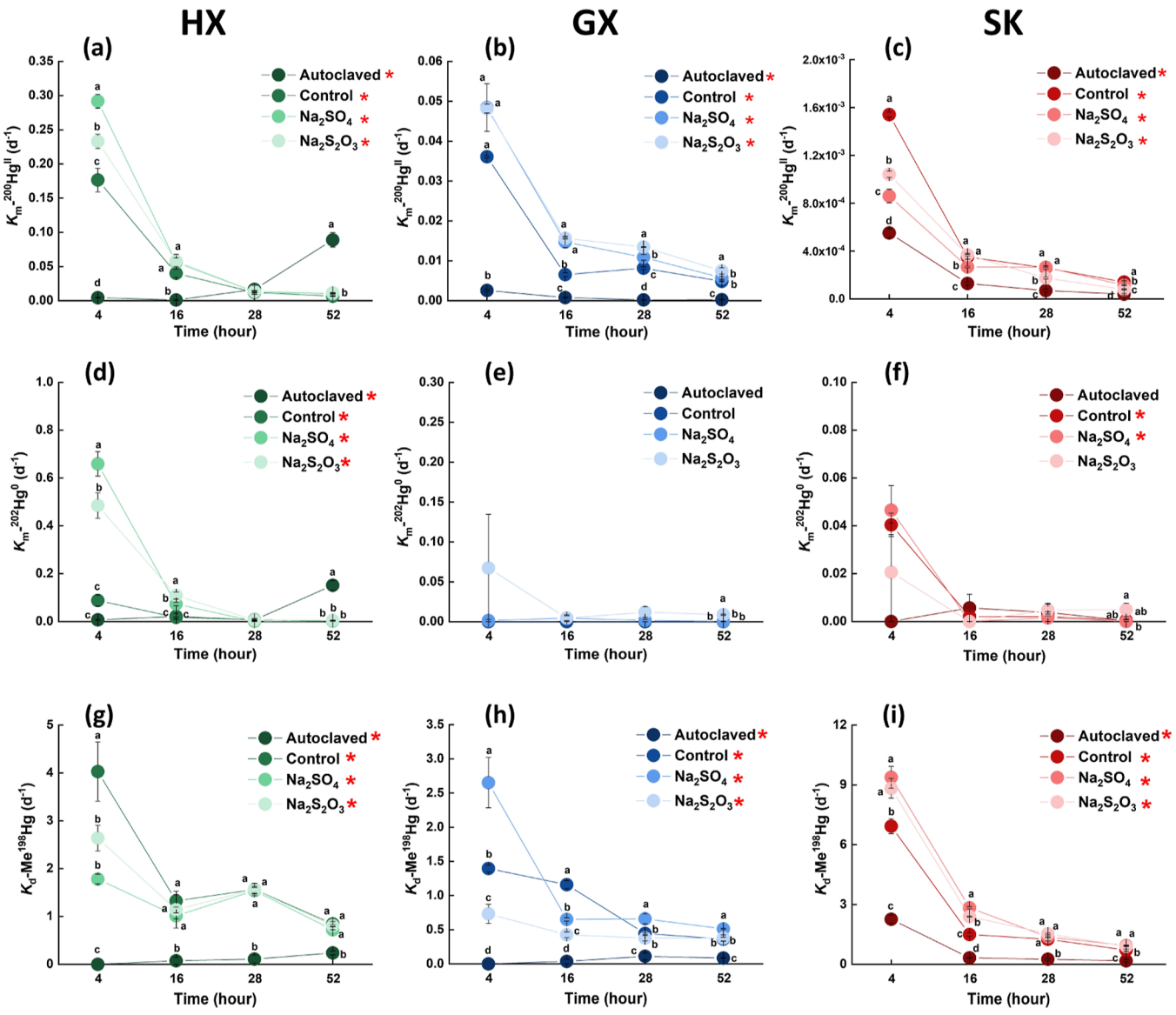

Figure 1. Methylation rate constants for $^{200}Hg^{2+}$ [K_m-$^{200}Hg^{2+}$, (a−c)], methylation rate constants for $^{202}Hg^0$ [K_m-$^{202}Hg^0$, (d−f)], and demethylation rate constants for $Me^{198}Hg$ [K_d-$Me^{198}Hg$, (g−i)] as a function of time at the three sites (HX, GX, and SK) across the different treatments. Error bars indicate the standard error (±SE) for replicates (n = 3). Different lowercase letters indicate that the differences between the treatments at each time point are significant (one-way ANOVA $p < 0.05$). Missing lowercase letters indicate no significant difference between treatments. "*" after the legend suggests that the differences within each treatment at different times are significant (t-test $p < 0.05$).

The concentrations of generated Me^iHg and $^iHg^0$ (i = 198, 200, and 202) were quantified by external calibrations[50] (Figure S2). The methylation rate constants [K_m-$^{200}Hg^{II}$ (d^{-1}) and K_m-$^{202}Hg^0$ (d^{-1})], demethylation rate constant [K_d-$Me^{198}Hg$ (d^{-1})], and volatilization rate constants [K_v-$Me^{198}Hg$ (d^{-1}) and K_v-$^{200}Hg^{II}$ (d^{-1})] were calculated from [Me^iHg], [$^iHg^0$] (i = 198, 200, and 202), and the amounts of spiked Hg tracers using an irreversible pseudo-first-order model.[52] Meanwhile, the ratios of produced MeHg to spiked inorganic Hg tracers [$Me^{200}Hg/^{200}Hg^{II}$ (%) and $Me^{202}Hg/^{202}Hg^0$ (%)], the ratio of MeHg losses to spiked MeHg tracer [$Me^{198}Hg$ demethylation (%)], and the ratios of produced purgeable Hg^0 to spiked Hg tracers [$^{200}Hg^0/^{200}Hg^{2+}$ (%) and $^{198}Hg^0/Me^{198}Hg$ (%)] were also obtained. The calculation details and assumptions made for the irreversible pseudo-first-order model are shown in Text S6. It should be noted that linear approximations may underestimate the rate constants in Hg transformation due to the presence of reversible reactions (e.g., demethylation),[53] adsorption, and precipitation of spiked Hg tracers.[54] Therefore, the rate constants obtained from this study may not be suitable for comparison with other works using different approaches. Similarly, using the measured purgeable Hg^0 may underestimate Hg^{II} reduction due to the potential existence of non-purgeable Hg^0 (e.g., immobilized by solid phases).[55,56] However, all purgeable Hg^0 was produced from Hg reduction; therefore, Hg volatilization was used in this study to represent Hg reduction.

2.5. QA/QC and Statistics. The certified reference material (CRM) ERM-CC580 was used, and the MeHg recovery measurement for CRM ranged from 76.2 to 108.4%, with an average of 85.2 ± 9.07% (n = 26), which is comparable with previous studies.[7,16,22,25,46,49] Duplicates were added every 10 samples during measurement, and the relative standard

https://doi.org/10.1021/acs.est.3c02676
Environ. Sci. Technol. 2023, 57, 8149−8160

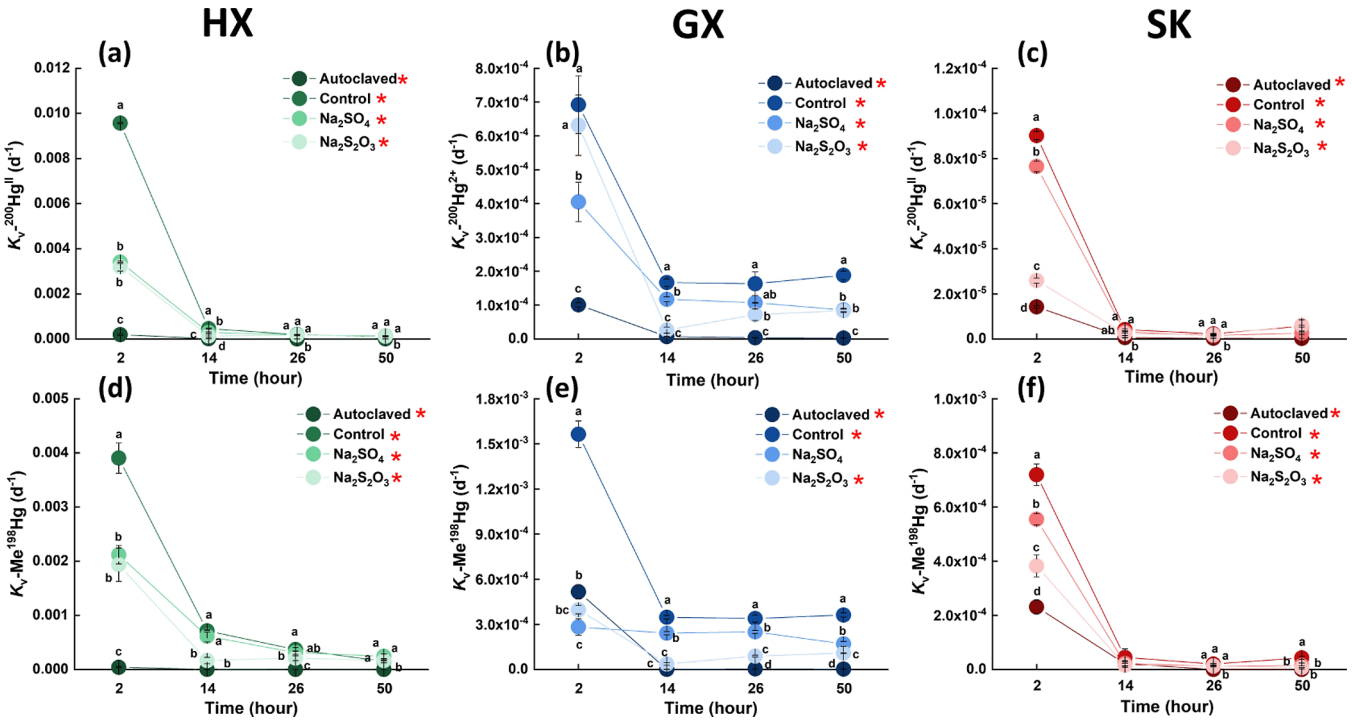

Figure 2. Volatilization rate constants for $^{200}Hg^{II}$ [K_v-$^{200}Hg^{II}$, (a–c)] and $Me^{198}Hg$ [K_v-$Me^{198}Hg$, (d–f)] as a function of time at the three sites (HX, GX, and SK) across the different treatments. Error bars indicate the standard error (±SE) for replicates (n = 3). Different lowercase letters indicate that the differences between the treatments at each time point are significant (one-way ANOVA $p < 0.05$). "*" after the legend indicates that the differences within each treatment at different times are significant (t-test $p < 0.05$).

deviation (RSD %) of duplicates is <10%. The instrument detection limits for Hg by using inductively coupled plasma–mass spectrometry is 10 pg. Data are presented as the mean ± standard error (SE). Group differences were assessed by t-tests and one-way ANOVA with Duncan's post hoc test using SPSS 23.0 (IBM, IL, USA). Statistical significance (p) was set at <0.05 (two-tailed).

3. RESULTS

3.1. Variations in Major Redox Couples and Soil DOM. Redox couples (HS^-–SO_4^{2-}, NH_4^+–NO_3^-, and Fe^{2+}–Fe^{3+}) were measured to show the redox conditions during incubation. The concentrations of NH_4^+ in the liquid phases of all paddy slurries were 2–3 orders of magnitude higher than those of NO_3^-; the highest NO_3^- concentrations were observed in the autoclaved treatments (Figure S3). Higher Fe^{2+} percentages in total Fe (Fe^{2+} + Fe^{3+}) were found in the two S treatments, as compared to the control treatment, at all sites ($p < 0.05$, Figure S4). Similar distribution patterns of SO_4^{2-} were found in the Na_2SO_4 and $Na_2S_2O_3$ treatments at sites HX and SK (Figure S5). The concentrations of sulfide (HS^-) at all sites were 3 orders of magnitude lower than those of SO_4^{2-} (Figure S5). It is noted that some large variations of Fe^{2+}, Fe^{3+}, and NO_3^- were observed in the autoclaved samples, and proper explanations are in the Text S7. The concentrations of soil DOM (represented by dissolved organic carbon, DOC) varied across the different sites ($p < 0.05$, Figure S6) but were similar among the different treatments at a given site ($p > 0.05$, Figure S6). UV–vis absorption and fluorescence spectra were used to characterize the compositional structure of DOM. Similarly, for almost all spectral indices [i.e., $SUVA_{254}$, $S_{275-295}$, a(355), fluorescence peaks, HIX, and BIX], there were no differences among the treatments (Figure S7). The only differences were as follows. First, higher intensities of fluorescence peak A ($p < 0.05$, Figure S7d) and peak C ($p < 0.05$, Figure S7e) were observed in the S addition treatments (i.e., both Na_2SO_4 and $Na_2S_2O_3$ treatments) as compared to the control at site SK. Second, at site GX, lower intensities of fluorescence peak B ($p < 0.05$, Figure S7f) and peak T ($p < 0.05$, Figure S7g) were observed in the S addition treatments as compared to the control.

3.2. Copy Numbers of the *hgcA*, *merA*, *merB*, *dsrB*, and *soxB* Genes and Hg-Methylating Communities. Copies of the *mer* operon (*merA* and *merB*) were below the detection limit in all treatments at all sites [real-time threshold cycle (C_T) > 31]. Significantly lower copies of *hgcA*, *dsrB*, and *soxB* were found in the autoclaved samples compared to the other treatments ($p < 0.05$, Figure S8). At site GX, the control treatment exhibited more *hgcA* genes than the two S treatments ($p < 0.05$, Figure S8b), while the opposite trend was observed at site SK ($p < 0.05$, Figure S8c). A distribution pattern similar to that of *hgcA* was found for *dsrB* at sites GX and SK (Figure S8e,f). More copies of the *soxB* gene in the $Na_2S_2O_3$ treatment were observed at the three sites, as compared to those in the Na_2SO_4 treatment ($p < 0.05$, Figure S8g–i). The *hgcA* gene amplicon sequencing revealed that the relative abundances of sulfate-reducing bacterium (SRB) methylators (i.e., SRB carrying the *hgcA* gene) in the S addition treatments at sites HX and GX were 1.04–1.56 and 1.27–1.82 times higher than that in the control, respectively ($p > 0.05$). The identified major SRB methylators were *Peptococcaceae*, *Desulfovibrionaceae*, and *Desulfobulbaceae* (Figure S9b). The search of the metagenomic data for homologues of *hgcA* revealed more SRB methylators in the S addition treatments than in the control at site HX (23.5% higher in

https://doi.org/10.1021/acs.est.3c02676
Environ. Sci. Technol. 2023, 57, 8149–8160

sulfate treatment and 17.5% higher in thiolsulfate treatment, Figure S9d).

3.3. Methylation of $^{200}Hg^{II}$ and $^{202}Hg^{0}$. The methylation rate constants, K_m-$^{200}Hg^{II}$ (d^{-1}) and K_m-$^{202}Hg^{0}$ (d^{-1}), show the methylation of spiked $^{200}Hg^{II}$ and $^{202}Hg^{0}$, respectively (Figure 1). The variation trend in K_m-$^{200}Hg^{II}$ was the same at all sites, with a sharp decrease from 4 to 16 h and a slight decrease thereafter; the autoclaved treatment at site HX was the only exception. However, the ranges of K_m-$^{200}Hg^{II}$ among the study sites differed greatly. The highest values of K_m-$^{200}Hg^{II}$ at sites HX, GX, and SK were all observed at the 4th h, with values of 0.29 ± 0.01 d^{-1} (in the Na_2SO_4 treatment, $p < 0.05$, Figure 1a), 0.048 ± 0.006 d^{-1} (in both the Na_2SO_4 and $Na_2S_2O_3$ treatments, $p < 0.05$, Figure 1b), and 0.0015 ± 0.00002 d^{-1} (in the control treatment, $p < 0.05$, Figure 1c), respectively. The ratios of produced $Me^{200}Hg$ to spiked $^{200}Hg^{II}$ [$Me^{200}Hg/^{200}Hg^{II}$ (%)] and the $Me^{200}Hg$ concentrations during incubation are shown in Figures S10 and S11, respectively. The S treatments yielded more production of $Me^{200}Hg$ than the control treatment at sites HX and GX ($p < 0.05$, Figure S11), and significantly higher $Me^{200}Hg$ was observed in the $Na_2S_2O_3$ treatment at site GX than in the Na_2SO_4 treatment (at the 52nd h, $p < 0.05$, Figure S11b).

The formation of $Me^{202}Hg$ from spiked $^{202}Hg^{0}$ reflects the methylation of $^{202}Hg^{0}$. At site HX, the highest K_m-$^{202}Hg^{0}$ was found at the 4th h in the Na_2SO_4 treatment (0.66 ± 0.05 d^{-1}, $p < 0.05$), followed by the $Na_2S_2O_3$ treatment (0.49 ± 0.05 d^{-1}, $p < 0.05$) and then the control and autoclaved treatments ($p < 0.05$, Figure 1a). Correspondingly, 10.98 ± 0.85 and 8.08 ± 0.89% of spiked $^{202}Hg^{0}$ were transformed to $Me^{202}Hg$ in the Na_2SO_4 and $Na_2S_2O_3$ treatments, respectively, at site HX (Figure S10d). At sites GX and SK, more $Me^{202}Hg$ was produced in the $Na_2S_2O_3$ treatment than in the other treatments (1.90 ± 0.17% for GX and 1.07 ± 0.59% for SK, $p < 0.05$, Figure S10e,f).

3.4. Demethylation of $Me^{198}Hg$. All $Me^{198}Hg$ tracers yielded significant degradation over time, except in the autoclaved treatments (Figure 1). At site HX, there were no significant differences in K_d-$Me^{198}Hg$ among the control, Na_2SO_4, and $Na_2S_2O_3$ treatments across the whole time series, with the exception of K_d-$Me^{198}Hg$ in the control treatment (4.03 ± 0.62 d^{-1}) at the 4th h. At sites GX and SK, the S-amended treatments yielded higher K_d-$Me^{198}Hg$ values than the control treatment at the end of incubation (the Na_2SO_4 treatment in GX and both the Na_2SO_4 and $Na_2S_2O_3$ treatments in SK) ($p < 0.05$, Figure 1h,i). Although demethylation of $Me^{198}Hg$ was also observed in the autoclaved treatments, it was significantly lower than that observed in the other treatments ($p < 0.05$, Figures S11d–f), suggesting that microbially mediated demethylation of MeHg is predominant in paddy soils.

3.5. Reduction of $^{200}Hg^{II}$ and Formation of $^{198}Hg^{0}$ from $Me^{198}Hg$. The volatilization rate constants, K_v-$^{200}Hg^{II}$ (d^{-1}) and K_v-$Me^{198}Hg$ (d^{-1}), show the formation of purgeable $^{200}Hg^{0}$ and $^{198}Hg^{0}$ by the reduction of spiked $^{200}Hg^{II}$ and $Me^{198}Hg$, respectively (Figure 2). Significantly higher amounts of purgeable $^{200}Hg^{0}$ and $^{198}Hg^{0}$ were detected in the non-autoclaved treatments than in the autoclaved samples at all sites (Figure S12). However, the ratios of produced purgeable $^{200}Hg^{0}$ and $^{198}Hg^{0}$ to spiked Hg tracers [$^{200}Hg^{0}/^{200}Hg^{II}$ (%) and $^{198}Hg^{0}/Me^{198}Hg$ (%)] were 1–2 orders of magnitude lower than those of $Me^{200}Hg/^{200}Hg^{II}$ (%) and $Me^{198}Hg$ demethylation (%) (Figures S10 and S13). In the initial period (2 h), K_v-$^{200}Hg^{II}$ in the control treatment was higher than those of the S-amended treatments (Na_2SO_4 and $Na_2S_2O_3$) at all sites ($p < 0.05$, except K_v-$^{200}Hg^{II}$ at site GX, Figure 2). Lower purgeable $^{200}Hg^{0}$ in the S treatments, as compared to the control treatment, was found at site GX across the entire study period ($p < 0.05$, Figure S12b) and at site HX in the first 14 h of incubation ($p < 0.05$, Figure S12a).

Similar to K_v-$^{200}Hg^{II}$, K_v-$Me^{198}Hg$ in the control treatment at the 2nd h was significantly higher than those of the S treatments at all sites ($p < 0.05$, Figure 2). However, a comparable purgeable $^{198}Hg^{0}$ mass was found between the control and S treatments across most of the incubation period at sites HX and SK (Figure S12d,f). Less purgeable $^{198}Hg^{0}$ mass was observed in the $Na_2S_2O_3$ treatment than the Na_2SO_4 treatment at site GX ($p < 0.05$, Figure S12e). It should be noted that some production of $^{198}Hg^{0}$ may be from $^{198}Hg^{II}$ reduction instead of from $Me^{198}Hg$ because the purity of our synthesized $Me^{198}Hg$ was 83.2%, which means that 16.8% of $^{198}Hg^{II}$ remained in the synthesized $Me^{198}Hg$. Therefore, the formation of $^{198}Hg^{0}$ only from $Me^{198}Hg$ was recalibrated according to the purity of $Me^{198}Hg$ and the fraction of conversion from $^{200}Hg^{II}$ to $^{200}Hg^{0}$ (Text S8). By subtracting $^{198}Hg^{0}$ originating from $^{198}Hg^{II}$, we found that 86.4 ± 11.6, 89.4 ± 10.4, and 97.1 ± 3.4% of $^{198}Hg^{0}$ were from $Me^{198}Hg$ at sites HX, GX, and SK, respectively. This confirms the transformation of $Me^{198}Hg$ to $^{198}Hg^{0}$. Thus, the recalibration procedure is necessary for accurately tracing the reduction of synthesized MeHg tracers; this has been ignored in previous studies.

3.6. Oxidation or Immobilization of $^{202}Hg^{0}$. The losses of spiked $^{202}Hg^{0}$ through purging suggest that purgeable $^{202}Hg^{0}$ is transformed to non-purgeable ^{202}Hg. Both oxidation and immobilization are responsible for the formation of non-purgeable ^{202}Hg. Rapid depletion of purgeable $^{202}Hg^{0}$ occurred in this study; more than 99.9% of spiked $^{202}Hg^{0}$ could not be purged out within 2 h (Figure S13g–i). S amendments significantly decreased the masses of purgeable $^{202}Hg^{0}$ at sites HX and GX when compared with the control treatment ($p < 0.05$, Figure S12g,h).

4. DISCUSSION

4.1. Mercury Transformation in Paddy Soils. Signals of isotope-enriched Hg tracers in the control and autoclaved treatments showed transformations (i.e., methylation, demethylation, reduction, and oxidation/immobilization) between different Hg species (Hg^{II}, MeHg, and Hg^{0}) in paddy soils.

Significantly lower $Me^{200}Hg$ production (Figures S10 and S11) in the autoclaved treatments compared to the other treatments suggests that abiotic methylation, if present at all, is negligible in paddy soils. Methylation of Hg^{II} (K_m-$^{200}Hg^{II}$) decreased by orders of magnitude over the Hg contamination gradient ([THg]: HX (0.15 ± 0.003 mg kg^{-1}) < GX (17.2 ± 1.7 mg kg^{-1}) < SK (609 ± 7 mg kg^{-1})), which is consistent with our previous findings.[22,25] Microbially mediated processes are likely the cause,[22,25] because (i) there were no differences in the soil texture and structure between the sites and (ii) Hg selective pressure can reshape the microbial community structure of paddy soils, altering the abundance of methylators or microbial helpers (e.g., syntrophic microorganisms) that support methylators.[57,58] Moreover, a lower concentration but more aromatic DOM (i.e., lower DOC but higher $SUVA_{254}$) was observed at site SK, as compared to sites HX and GX ($p <$

https://doi.org/10.1021/acs.est.3c02676
Environ. Sci. Technol. 2023, 57, 8149–8160

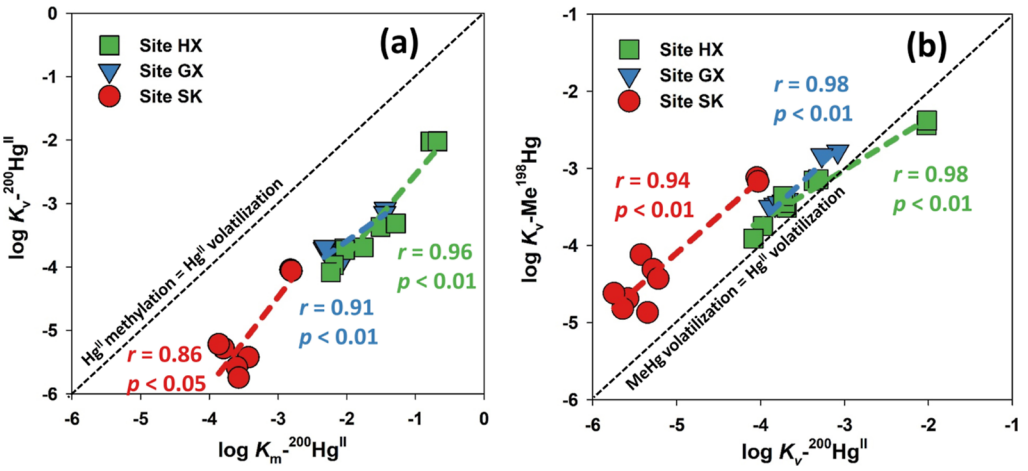

Figure 3. log K_m-$^{200}Hg^{II}$ vs log K_v-$^{200}Hg^{II}$ (a) and log K_v-$^{200}Hg^{II}$ vs log K_v-$Me^{198}Hg$ (b) at the three sites (HX, GX, and SK) in the control treatment. Dashed lines represent the 1:1 line between two variables.

0.05, Figures S6 and S7). This implies that DOM with a high humification degree inhibits microbially mediated Hg^{II} methylation. This is also supported by the observed negative correlations between K_m-$^{200}Hg^{II}$ and the humic-like characters of the DOM at all sites ($r = -0.58$ and $p < 0.05$ for K_m-$^{200}Hg^{II}$ vs peak A, $r = -0.75$ and $p < 0.01$ for K_m-$^{200}Hg^{II}$ vs peak C, and $r = -0.77$ and $p < 0.01$ for K_m-$^{200}Hg^{II}$ vs $SUVA_{254}$, Table S3). Typically, DOM with a lower molecular weight, less humic substances, and more autochthonous sources (e.g., low-molecular-weight organic acids, proteins, and sugars) can more readily fuel microbially mediated Hg^{II} methylation, as compared to highly aromatic or humic substances.[59]

Active methylation of $^{200}Hg^{II}$ (Figures 1a, S10a, and S11a) and increasing copies of the *hgcA* gene (Figure S8) were observed in the autoclaved treatment at site HX at the end of the period of incubation. This suggests potential microbial succession unaccounted for after autoclaving. An uncertain effect of autoclaving on the inhibition of bacterial activity has previously been reported, which is consistent with this observation.[22,60] A spread-plate experiment was conducted using autoclaved samples to test the activity of microorganisms (Text S9). No countable colony-forming units were identified, suggesting that the microorganisms responsible for the increase in the *hgcA* signal in the autoclaved samples are nonculturable with the selected growth medium. Moreover, we observed a significant correlation between methylation using either $^{200}Hg^{II}$ or $^{202}Hg^{0}$ as the substrate in the autoclaved treatment at site HX (Figure S14). This implies that both $^{202}Hg^{0}$ and $^{200}Hg^{II}$ can be methylated and their methylation processes are highly correlated. This is not surprising because Hg^{0} can be methylated after oxidation[61] in cultures of *Desulfovibrio desulfuricans* ND132[62,63] and *Geobacter sulfurreducens* PCA.[63,64] In this study, less than 0.1% of spiked $^{202}Hg^{0}$ was recovered as purgeable $^{202}Hg^{0}$ during incubation (i.e., dominated by non-purgeable ^{202}Hg, Figure S12g–i). The rapid formation of non-purgeable ^{202}Hg from spiked $^{202}Hg^{0}$ implies the rapid oxidization or solid-phase immobilization of $^{202}Hg^{0}$ in paddy soil slurries. Non-purgeable Hg^{0} can be present as Hg^{0} or Hg^{II} associated with particles.[56] However, with the presence of natural organic matter[65,66] and some anaerobic bacteria,[62,63] Hg^{0} can easily be oxidized to Hg^{II}. In particular, several recent studies have reported that particulate-bound Hg^{II} can also act as a bioavailable substrate fueling methylation.[67,68] Previously, Colombo et al.[62] and Hu et al.[63] reported the biotic oxidation of Hg^{0} through pure culture studies. The current results demonstrated that abiotic reactions likely dominate the oxidization of spiked $^{202}Hg^{0}$ due to the lower purgeable $^{202}Hg^{0}$ masses recovered from the autoclaved treatments, as compared to the other treatments ($p < 0.5$, Figure S12g–i). In this study, the spiked $^{202}Hg^{0}$ in paddy soils was likely oxidized to $^{202}Hg^{II}$ and then microbially methylated. Accordingly, both biotic oxidation[61−64] and abiotic oxidation[65,66] of Hg^{0} will provide Hg^{II} fuel for methylation. This observation supports the hypothesis that rapid redox recycling of Hg species contributes to Hg speciation resetting, forming bioavailable Hg^{II} at methylation sites.[69]

In addition to the coupled reactions of oxidization and methylation of Hg^{0} in paddy soils, the reduction of Hg^{II} was also co-varied with the methylation of Hg^{II}, as indicated by the significant correlation between log K_m-$^{200}Hg^{II}$ and log K_v-$^{200}Hg^{II}$ in the control treatment (Figure 3a). Historically, it was assumed that reduction competes with methylation for bioavailable Hg^{II} substrates; however, this view is rapidly changing, as Hg^{0} has been shown to be capable of serving as a substrate for methylation.[62,63] In this microcosm study, competition between methylation and reduction was also not observed due to the co-variation between K_m-$^{200}Hg^{II}$ and K_v-$^{200}Hg^{II}$ (Figure 3a). Lu et al.[70] identified a *merA*- and *merB*-containing iron-reducing bacterium capable of simultaneously methylating Hg^{II} and generating Hg^{0} through reductive demethylation of MeHg in anoxic conditions. Here, no significant correlation was observed between $^{200}Hg^{II}$ methylation (shown as K_m-$^{200}Hg^{II}$ or $Me^{200}Hg/^{200}Hg^{II}$ %) and $Me^{198}Hg$ demethylation (shown as K_d-$Me^{198}Hg$ and $Me^{198}Hg$ demethylation %), and the *merA* and *merB* genes were below the detection limit. This suggests that reductive demethylation of newly formed $Me^{200}Hg$ (via the *mer* operon) is not the likely mechanism responsible for the correlation between $^{200}Hg^{II}$ methylation and reduction. Rather, other pathways, such as the involvement of c-type cytochromes in Hg^{II} reduction[63] and/or photoheterotrophic or fermentative Hg^{II} reduction,[71] may exist in paddy soils. The former process depends on extracellular electron transfer, whereas the latter depends on the presence of fermentable carbon sources in the dark or stimulation of bacterial phototrophy in the presence of light.[69,71,72] However, the reduction of $^{200}Hg^{II}$ was 1−2 orders of magnitude lower

https://doi.org/10.1021/acs.est.3c02676
Environ. Sci. Technol. 2023, 57, 8149−8160

than the methylation of $^{200}Hg^{II}$ (Figures 3a, S11, and S12), suggesting a predominant role of methylation when compared with the reduction of Hg^{II} in paddy soils. It is also possible that the newly produced $^{200}Hg^0$ is rapidly re-oxidized to $^{200}Hg^{II}$ prior to being methylated to $Me^{200}Hg$ (i.e., avoiding the purge). This quick redox recycling step may favor $^{200}Hg^0$ accessibility and availability to methylators. As a result, rapid anoxic redox cycling, further away from the air/water interface, may maintain a pool of bioavailable Hg^{II}, albeit small, that sustains methylation. Nevertheless, over a large scale or long term, Hg reduction and its subsequent evasion may still contribute to the removal of Hg from rice paddy soils and, therefore, limit the formation of MeHg, especially in uncontaminated paddy soils (i.e., Hg^{II} methylation is constrained by the THg concentration). Therefore, it is critical to tease apart the importance of these two pathways for the proper management of paddy systems.

In this study, purgeable $^{198}Hg^0$ was detected from the spiked $Me^{198}Hg$ (Figure S12d−f), whereas the ratio of purgeable $^{198}Hg^0$ to the spiked $Me^{198}Hg$ ($^{198}Hg^0/Me^{198}Hg$ %) was 3−4 orders of magnitude lower than the $Me^{198}Hg$ demethylation % (Figures S10 and S13). The copy numbers of the *mer* operon genes (*merA* and *merB*), which mediate reductive demethylation,[73,74] were below the detection limit in the control treatment. In the absence of a broad-range *mer* operon (i.e., involved in both MeHg degradation and Hg^{II} reduction), *mer*-independent oxidative demethylation (OD) may be a significant mechanism underlying MeHg degradation in paddy soils.[75] Oxidative demethylation is a nonspecific co-metabolic process producing Hg^{II} and CO_2 and is commonly observed in anoxic conditions.[74,76] In this study, the correlations between K_v-$Me^{198}Hg$ and K_v-$^{200}Hg^{II}$ (Figure 3b) and between purgeable $^{198}Hg^0$ and $^{200}Hg^0$ (Figure S15) suggest that the formation of purgeable $^{198}Hg^0$ from $Me^{198}Hg$ is a two-step reaction: $Me^{198}Hg$ is oxidatively demethylated to $^{198}Hg^{II}$ and then reduced to $^{198}Hg^0$, likely using a pathway similar to $^{200}Hg^{II}$ reduction. The data points were located close to the log K_v-$Me^{198}Hg$: log K_v-$^{200}Hg^{II}$ = 1:1 line (Figure 3b), further supporting the control of $Me^{198}Hg$ degradation by mechanisms similar to or closely associated with $^{198}Hg^{II}$ reduction. Moreover, significant correlations were observed between the purgeable $^{200}Hg^0$ and $^{202}Hg^0$ masses at all sites (Figure S15), implying that the formation of Hg^0 from spiked $^{200}Hg^{II}$, $Me^{198}Hg$, and $^{202}Hg^0$ tracers is the same as Hg^{II} reduction. This further highlights that the formation of Hg^{II} may be a precondition for subsequent methylation and reduction. In addition, significant correlations between humic-like characters of DOM (i.e., humic-like compounds indicated by peak A and peak C and aromaticity indicated by $SUVA_{254}$) and K_v (i.e., both K_v-$Me^{198}Hg$ and K_v-$^{200}Hg^{II}$) were observed but were absent with K_d-$Me^{198}Hg$ (Table S3). This implies that humic fractions of soil DOM inhibited Hg^{II} reduction. This is the major mechanism explaining the inhibited transformation of MeHg to Hg^0 by humified DOM.

Partitioning of Fe between solid and aqueous phases plays a role in Hg transformation. This was evidenced by the significant correlations between the aqueous Fe concentration (i.e., Fe^{2+}+Fe^{3+}) and K_m-$^{200}Hg^{II}$ or K_v-$^{200}Hg^{II}$ in this study (Table S4). Research has demonstrated that reductive dissolution of Fe(oxyhydr)oxides may increase the bioavailability of previously adsorbed Hg^{II}.[24,26] However, the recrystallization from Fe(oxyhydr)oxides to Fe−S solids (e.g., FeS and FeS_2) may largely decrease the bioavailability of the released Hg^{II} from Fe(oxyhydr)oxides.[25,29] The influence of redox cycling of Fe in aqueous phases (Fe^{2+}−Fe^{3+} couple) on Hg transformation was absent in this microcosm study. More research on Fe redox cycling in both solid and aqueous phases, and its influence on Hg transformation, is needed in the future.

4.2. Role of Sulfate and Thiosulfate in Hg Transformation in Paddy Slurries. The influences of S addition on Hg methylation/demethylation were not only dependent on the S species but also on the study site (Figures 1 and 2, S11, and S12). The roles of S species in different Hg transformation processes raise two questions: (i) how does the S input influence Hg transformation in paddy soils? and (ii) do sulfate and thiosulfate affect the abovementioned processes to the same extent? These two questions are addressed below.

4.2.1. Hg Speciation Change- vs Microbial-Driven Hg Transformation under S Input Conditions. The bioavailability of Hg and the microbial community are recognized as important factors determining biotic Hg cycling in the natural environment.[20,77] However, it is still not clear whether S-dependent Hg transformation is regulated by Hg speciation (or mobility/bioavailability) or by changes in the microbial community structure and function in response to S species amendments. Recently, Li et al.[21] and Lei et al.[47] reported that an increase in Hg mobility, rather than changes in the structure and functional profiles of microbial methylators, triggers an enhancement of Hg methylation in S-amended paddy soils. Here, Hg speciation and the microbial community were found to play different roles in Hg methylation in S-treated paddy soils with different Hg contamination levels.

At sites (HX and GX) with low and moderate [THg] levels, opposing influences of S addition on Hg methylation and reduction were observed; the addition of Na_2SO_4 and $Na_2S_2O_3$ increased the formation of $Me^{200}Hg$ but decreased the formation of $^{200}Hg^0$ from $^{200}Hg^{II}$ ($p < 0.05$, Figures 1, 2, and S10−S13). If the bioavailability of Hg is increased, it is expected that S addition would promote Hg^{II} methylation and reduction synchronously, especially given the presence of the co-varied methylation and reduction of Hg^{II} as discussed above (Figure 3a). Despite the very limited experimental evidence, the uptake of Hg^{II} species by Hg methylators and Hg reducers is assumed to be comparable. In our previous study, SRBs were confirmed to be the dominant Hg^{II} methylators at site HX and one of the Hg^{II} methylators at site GX.[22] Here, both Na_2SO_4 and $Na_2S_2O_3$ provided SO_4^{2-}, thus fueling the SRB following oxidization or disproportionation of $S_2O_3^{2-}$.[78−80] Therefore, the SRB-mediated Hg^{II} methylation at sites HX and GX was likely promoted. In particular, higher SO_4^{2-} concentrations ($p < 0.05$, Figure S5a) and copy numbers of the *dsrB* gene ($p < 0.05$, Figure S8d) in the S treatments compared to the control treatment were identified at site HX. At site GX, however, S addition significantly reduced the abundance of the *dsrB* gene ($p < 0.05$, Figure S8e), and this was closely correlated with *hgcA* gene copies (Figure S16). This implies that in addition to SRB, other microorganisms are also involved in Hg^{II} methylation, and SO_4^{2-} might be a limiting factor for methylation at site GX.[22] In addition, more SRB methylators were observed in the S addition treatments compared to the control at sites HX and GX through either *hgcA* gene amplicon sequencing or metagenomic analysis (Figure S9), which provides direct evidence that the activity of SRB methylators was promoted by adding both sulfate and thiolsulfate. Among all the identified SRB methylators, *Desulfomonile* is likely a key SRB genus associate with Hg^{II} methylation at sites HX and GX

https://doi.org/10.1021/acs.est.3c02676
Environ. Sci. Technol. 2023, 57, 8149−8160

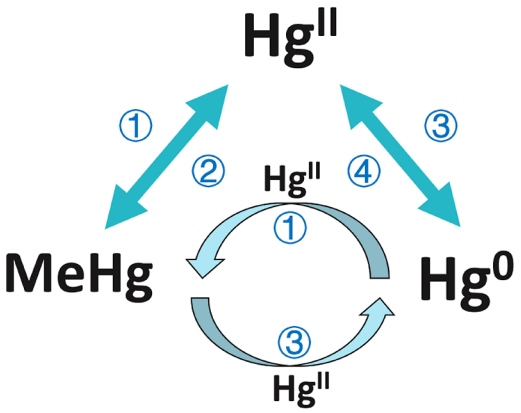

Hg Transformations		Fraction of conversion (%)			Biotic or abiotic processes
		Site HX	Site GX	Site SK	
(1) Methylation	$Hg^{II} \rightarrow MeHg$	1.43 ± 0.10 %	1.05 ± 0.03 %	0.31 ± 0.02 ‰	
	$Hg^{0} \rightarrow Hg^{II} \rightarrow MeHg$	0.44 ± 0.11 %	0 %	0.11± 0.11 %	e⁻
(2) Demethylation	$MeHg \rightarrow Hg^{II}$	83.8 ± 1.78 %	54.3 ± 2.63 %	78.4 ± 2.57 %	
(3) Reduction	$Hg^{II} \rightarrow Hg^{0}$	0.20 ± 0.02 ‰	0.39 ± 0.03 ‰	0.012 ± 0.001 ‰	
	$MeHg \rightarrow Hg^{II} \rightarrow Hg^{0}$	0.31 ± 0.06 ‰	0.75 ± 0.03 ‰	0.089 ± 0.012 ‰	
(4) Oxidation/ immobilization	$Hg^{0} \rightarrow Hg^{II}$/non-purgeable Hg^{0}	> 99.9 %	> 99.9 %	> 99.9 %	e⁻

Biotic process Abiotic process

Figure 4. Schematic diagram illustrating Hg cycling in paddy soils and transformation rates of each process. Fractions of conversion are from Figures S10 and S13.

under S addition, due to its significant co-variation with log K_m-$^{200}Hg^{II}$ (Figure S17).

Inhibition of $^{200}Hg^{II}$ reduction under S addition at sites HX and GX ($p < 0.05$, Figures 2 and S12) could be interpreted in two ways. (i) S addition promotes both Hg^{II} and Hg^0 methylation. The rapid redox cycling of Hg^0 makes it a bioavailable substrate for methylation (discussed above) which, therefore, reduces the amount of purgeable Hg^0. (ii) Exogenous S addition may break the balance between Hg^{II} methylators (i.e., SRB) and Hg^{II} reducers, thereby reducing the activity of Hg^{II} reducers. However, the communities of Hg^{II} reducers in this study remain unknown (i.e., *merA*-independent reducers), and more research is needed.

At the most contaminated site (SK, with the highest [THg]), Hg^{II} methylation and reduction were hampered, whereas demethylation of MeHg was promoted in the S-treated paddy soils when compared with the control treatment at site SK (Figures 1, 2, S11, and S12). It should be noted that a much higher NO_3^- concentration (1−3 orders of magnitude higher than those at sites HX and GX) was observed in the autoclaved treatment compared to the other treatments at site SK ($p < 0.05$, Figure S1c). This suggests that significant dissimilatory reduction of NO_3^- occurred in the presence of microorganisms.[81] The reduction of a large amount of NO_3^- may deplete electron donors for Hg^{II} methylation (e.g., sulfate reduction, iron reduction, and methanogenesis processes) and Hg^{II} reduction,[82−84] as evidenced by the higher SO_4^{2-} ($p < 0.05$, Figure S5) and lower Fe^{2+} ($p < 0.05$, Figure S6) concentrations at the end of incubation when compared with sites HX and GX. In addition, our previous work revealed that methanogens are involved in MeHg formation at site SK.[22] In this study, among the community of Hg methylators, higher relative abundances of *Methanothrix* and *Methanoregula*, carrying *hgcA* genes, were observed at site SK as compared to sites HX and GX (Figure S9c). Therefore, adding SO_4^{2-} will bring more competition for substrates between SRB and methanogens. In particular, the formation of CH_4 is thermodynamically more difficult than the reduction of SO_4^{2-} (i.e., a lower Eh is required).[85] In the matter of MeHg demethylation, promotion of SRB by the addition of SO_4^{2-} sources may facilitate SRB-mediated OD, since SRB is one of the major players in OD,[74,86] and OD was the dominant pathway for MeHg degradation in this study. The role of DOM in Hg transformation among different treatments is limited, due to the comparable optical properties for most of the indices (Figure S6). It is worth mentioning that consumption of protein-like compounds under the S addition treatments was observed at site GX (lower peak *B* and peak *T* than control, $p < 0.05$, Figure S6e,f). This partly explains the promoted activity of microorganisms (e.g., SRB) under sulfate and thiosulfate addition because the protein-like substances could be utilized preferentially by microorganisms.[87]

The evidence discussed above suggests that the increased production of MeHg is likely attributed to the facilitated activity of Hg^{II} methylators under the exogenous S input. Hg transformations are more sensitive to microorganisms involved in S cycling than Hg speciation changes regulated by reduced S species. S amendments affect the microbial community structure and functional profile of Hg methylators by directly supplying metabolic substrates (i.e., SO_4^{2-} for SRB) or amplifying the competition for metabolic substrates.

4.2.2. Sulfate vs Thiosulfate. Sulfate is a terminal electron acceptor, and thiosulfate is one of the major intermediates in S redox cycling.[78,80,88,89] In this study, the rates and magnitudes of Hg transformations in the S treatments were dependent on the S species (i.e., SO_4^{2-} and $S_2O_3^{2-}$).

Previous studies have reported that Hg^{II} can bind with $S_2O_3^{2-}$ and form bioavailable Hg−S_2O_3 complexes [e.g., $Hg(S_2O_3)_2^{2-}$ and $Hg(S_2O_3)_3^{4-}$],[90−93] which may be the mechanism underlying $Na_2S_2O_3$ addition-promoted methylation. However, the current results appear to suggest a different scenario. We suspect that the added $S_2O_3^{2-}$ was unstable and readily transformed into SO_4^{2-} rather than forming Hg−S_2O_3 complexes; this is evidenced by the similar SO_4^{2-} concentrations to those in the Na_2SO_4 treatment (Figure S5a−c). Furthermore, our modeling exercise (Visual MINTEQ, Text S10) predicted that the speciation of Hg^{II} was dominated by Hg-sulfide complexes [e.g., HgS_2H^-, $Hg(SH)_2^0$, and HgS_2^{2-}, Figure S18]; Hg−S_2O_3 complexes, if present at all, were negligible when sulfides were present in the paddy soils. In addition to Hg speciation changes, the prolonged supply of SO_4^{2-} to Hg^{II} methylators in the $Na_2S_2O_3$ treatment is probably another mechanism for the enhanced Hg^{II} methylation. Rapid depletion of SO_4^{2-} was found in the Na_2SO_4 treatment. However, in the $Na_2S_2O_3$ treatment, $S_2O_3^{2-}$ and its acid decomposition products (i.e., SO_3^{2-} and S^0)[79] involved in

https://doi.org/10.1021/acs.est.3c02676
Environ. Sci. Technol. 2023, 57, 8149−8160

disproportionation also continuously supplied SO_4^{2-}. These reactions are considered to be typical inorganic fermentations and are independent of external reductants or oxidants.[94] In the current study, the formation of SO_4^{2-} at site GX was slower than at sites HX and SK, suggesting that the oxidation of $S_2O_3^{2-}$ was likely concomitant with the reduction of SO_4^{2-} in the $Na_2S_2O_3$ and Na_2SO_4 treatments, respectively (Figure S5b). Moreover, higher abundances of S-oxidizing bacteria (*soxB* gene) were observed in the $Na_2S_2O_3$ treatments than the Na_2SO_4 treatments. In particular, copies of the *soxB* gene were negatively correlated with $[HS^-]$ at site GX ($r = -0.87$ and $p < 0.01$), which further confirms the capability of $S_2O_3^{2-}$ to replenish SO_4^{2-} through S oxidation (Figure S8g–i). This highlights that the role of S-oxidizing bacteria in SRB-mediated Hg methylation should be given more attention. In summary, the mechanisms of $S_2O_3^{2-}$- and SO_4^{2-}-regulated Hg^{II} methylation are partly different. Both can enhance SO_4^{2-} supply for Hg^{II} methylation, albeit at different rates. Therefore, the kinetics of SO_4^{2-} production or microbial SO_4^{2-} utilization influenced by the $S_2O_3^{2-}$ input can more likely explain the greater formation of MeHg in the $Na_2S_2O_3$ treatment. This deserves further study in the future. Although this study was not able to provide evidence as to how Hg speciation changes influence Hg methylation under S addition, this should not be ignored, especially in redox-fluctuation paddy soils.

5. ENVIRONMENTAL IMPLICATIONS

In addition to the widely accepted Hg^{II} methylation and MeHg demethylation, this study provides direct evidence of Hg^{II} reduction, Hg^0 oxidation/immobilization, Hg^0 methylation, and the formation of Hg^0 from MeHg in paddy soils (Figure 4). These processes are biotically mediated, with only one exception being that Hg^0 oxidation/immobilization is mainly mediated by abiotic processes. The finding that dark reduction of Hg^{II} occurs through a biotically mediated process in paddy soils further highlights the role of microbial reduction of Hg^{II} in this environmental media. Interestingly, Hg^0 from the dark reduction of Hg^{II} can be methylated upon re-oxidation. The comparable K_m-$^{202}Hg^0$ and K_m-$^{200}Hg^{II}$ values further imply the rapid redox recycling of Hg species, fueling methylation. The transformation of MeHg to Hg^0 is attributed to oxidative demethylation coupled with reduction, instead of reductive demethylation (RD), in flooded paddy soils; RD may occur during the drying period (air-exposed) of rice-growing in paddy soils.[74] These findings highlight that (i) biotically mediated dark reduction of Hg^{II} followed by re-oxidation is also a source of Hg^{II} methylation in flooded paddy soils; this has been largely overlooked previously in redox fluctuating environments; and (ii) transformation processes for different Hg species (Hg^0, Hg^{II}, and MeHg) in paddy soils are closely associated with each other. In addition to Hg^{II} reduction and methylation as mentioned above, MeHg may also be a source of Hg^0 emission into the atmosphere through oxidative demethylation and then reduction. This highlights the continuous and dynamic nature of Hg transformation in paddy soils.

Sulfate reduction and the formation of reduced S species (sulfide, elemental sulfur, polysulfides, etc.) have long been considered as factors influencing Hg transformation due to the role of the SRB in Hg^{II} methylation[38,89] and speciation changes of Hg.[29−31] However, this study implies that the oxidation of reduced S species by S-oxidizing bacteria is also an important process in Hg^{II} methylation. The likely mechanisms are (i) to provide more sulfate and (ii) to change the rate of sulfate supply in sulfate reduction. Therefore, SRB-mediated Hg^{II} methylation is not only influenced by the quantity of sulfate but also controlled by the kinetics of sulfur species transformations, warranting additional work to fully explore their connection to Hg methylation.

■ ASSOCIATED CONTENT

Supporting Information

The Supporting Information is available free of charge at https://pubs.acs.org/doi/10.1021/acs.est.3c02676.

Additional descriptions of sampling sites and sample collection; preparation of Hg tracers; preparation of paddy slurry; subsampling and measurements; calculation for ambient and isotope-enriched Hg signals; fraction of conversion and corresponding rate constants in Hg transformation; explanation for Fe^{2+}, Fe^{3+}, and NO_3^- variations; recalculation of produced $^{198}Hg^0$ from $Me^{198}Hg$; spread-plate experiment; MINTEQ modeling; amounts of spiked Hg tracers; primers used in qPCR; correlation between optical properties of DOM and Hg transformation rate constants; correlation between Fe species and Hg transformation rate constants; comparison of matrix-based deconvolution approach and the simplified approach; quality control for the external standard method; concentrations of NO_3^-/NH_4^+, Fe^{2+}/Fe^{3+}, SO_4^{2-}/HS^-, and DOC; optical properties of DOM; copy numbers of *hgcA*, *dsrB*, and *soxB* genes; mercury-methylating communities; concentrations of $Me^{198}Hg$, $Me^{200}Hg$, and $Me^{202}Hg$; masses of purgeable $^{198}Hg^0$, $^{200}Hg^0$, and $^{202}Hg^0$; ratio of produced MeHg or Hg^0 from spiked Hg tracers; log K_m-$^{200}Hg^{II}$ versus log K_m-$^{202}Hg^0$; log *hgcA* versus log *dsrB*; correlations among purgeable $^{198}Hg^0$, $^{200}Hg^0$, and $^{202}Hg^0$ masses; log K_m-$^{200}Hg^{II}$ versus relative abundance of SRB methylators; and speciation of Hg^{II} (PDF)

■ AUTHOR INFORMATION

Corresponding Author

Bo Meng − *State Key Laboratory of Environmental Geochemistry, Institute of Geochemistry, Chinese Academy of Sciences, Guiyang 550002, China;* orcid.org/0000-0002-7827-8673; Phone: +86-851-84396920; Email: mengbo@vip.skleg.cn; Fax: +86-851-85891721

Authors

Jiang Liu − *State Key Laboratory of Environmental Geochemistry, Institute of Geochemistry, Chinese Academy of Sciences, Guiyang 550002, China*

Ji Chen − *State Key Laboratory of Environmental Geochemistry, Institute of Geochemistry, Chinese Academy of Sciences, Guiyang 550002, China; College of Chemical Engineering, Huaqiao University, Xiamen 361021, China;* orcid.org/0000-0002-3385-1149

Alexandre J. Poulain − *Biology Department, University of Ottawa, Ottawa ON K1N 6N5, Canada;* orcid.org/0000-0002-0488-3993

Qiang Pu − *State Key Laboratory of Environmental Geochemistry, Institute of Geochemistry, Chinese Academy of Sciences, Guiyang 550002, China*

Zhengdong Hao − *State Key Laboratory of Environmental Geochemistry, Institute of Geochemistry, Chinese Academy of*

Sciences, Guiyang 550002, China; University of Chinese Academy of Sciences, Beijing 100049, China

Xinbin Feng − *State Key Laboratory of Environmental Geochemistry, Institute of Geochemistry, Chinese Academy of Sciences, Guiyang 550002, China;* orcid.org/0000-0002-7462-8998

Complete contact information is available at: https://pubs.acs.org/10.1021/acs.est.3c02676

Notes

The authors declare no competing financial interest.

■ ACKNOWLEDGMENTS

This research was supported by the National Natural Science Foundation of China (42022024, 41931297, 41921004, and 42107442), the CAS "Light of West China" program, Guizhou Provincial 2020 Science and Technology Subsidies (no GZ2020SIG), and the Guizhou Provincial Natural Science Foundation (Qian- Ke-He-Ji-Chu ZK [2023] Yi ban 474). We thank Kun Zhang for his help in the sample analysis. We also thank Dr. Tao Jiang, Siqi Zhang, and Sihua Zhu, all from Southwest University, for their valuable help in DOM analysis and discussion about the manuscript revision.

■ REFERENCES

(1) St. Louis, V. L.; Rudd, J. W. M.; Kelly, C. A.; Bodaly, R. A. D.; Paterson, M. J.; Beaty, K. G.; Hesslein, R. H.; Heyes, A.; Majewski, A. R. The Rise and Fall of Mercury Methylation in an Experimental Reservoir. *Environ. Sci. Technol.* **2004**, *38*, 1348−1358.

(2) Schartup, A. T.; Balcom, P. H.; Soerensen, A. L.; Gosnell, K. J.; Calder, R. S. D.; Mason, R. P.; Sunderland, E. M. Freshwater Discharges Drive High Levels of Methylmercury in Arctic Marine Biota. *Proc. Natl. Acad. Sci. U.S.A.* **2015**, *112*, 11789−11794.

(3) Zhao, L.; Anderson, C. W. N.; Qiu, G.; Meng, B.; Wang, D.; Feng, X. Mercury Methylation in Paddy Soil: Source and Distribution of Mercury Species at a Hg Mining Area, Guizhou Province, China. *Biogeosciences* **2016**, *13*, 2429−2440.

(4) Zhao, L.; Qiu, G.; Anderson, C. W. N.; Meng, B.; Wang, D.; Shang, L.; Yan, H.; Feng, X. Mercury Methylation in Rice Paddies and Its Possible Controlling Factors in the Hg Mining Area, Guizhou Province, Southwest China. *Environ. Pollut.* **2016**, *215*, 1−9.

(5) Liu, J.; Jiang, T.; Wang, F.; Zhang, J.; Wang, D.; Huang, R.; Yin, D.; Liu, Z.; Wang, J. Inorganic Sulfur and Mercury Speciation in the Water Level Fluctuation Zone of the Three Gorges Reservoir, China: The Role of Inorganic Reduced Sulfur on Mercury Methylation. *Environ. Pollut.* **2018**, *237*, 1112−1123.

(6) Liem-Nguyen, V.; Skyllberg, U.; Björn, E. Methylmercury Formation in Boreal Wetlands in Relation to Chemical Speciation of Mercury(II) and Concentration of Low Molecular Mass Thiols. *Sci. Total Environ.* **2021**, *755*, 142666.

(7) Zhou, X.; Qu, X.; Yang, Z.; Zhao, J.; Hao, Y.; Feng, J.; Huang, Q.; Liu, Y. Increased Water Inputs Fuel Microbial Mercury Methylation in Upland Soils. *J. Hazard. Mater.* **2022**, *439*, 129578.

(8) Feng, X.; Li, P.; Qiu, G.; Wang, S.; Li, G.; Shang, L.; Meng, B.; Jiang, H.; Bai, W.; Li, Z.; Fu, X. Human Exposure to Methylmercury through Rice Intake in Mercury Mining Areas, Guizhou Province, China. *Environ. Sci. Technol.* **2008**, *42*, 326−332.

(9) Zhang, H.; Feng, X.; Larssen, T.; Qiu, G.; Vogt, R. D. In Inland China, Rice, Rather than Fish, Is the Major Pathway for Methylmercury Exposure. *Environ. Health Perspect.* **2010**, *118*, 1183−1188.

(10) Qiu, G.; Feng, X.; Li, P.; Wang, S.; Li, G.; Shang, L.; Fu, X. Methylmercury Accumulation in Rice (*Oryza Sativa L.*) Grown at Abandoned Mercury Mines in Guizhou, China. *J. Agric. Food Chem.* **2008**, *56*, 2465−2468.

(11) Zhang, H.; Feng, X.; Larssen, T.; Shang, L.; Li, P. Bioaccumulation of Methylmercury versus Inorganic Mercury in Rice (Oryza Sativa L.) Grain. *Environ. Sci. Technol.* **2010**, *44*, 4499−4504.

(12) Meng, B.; Feng, X.; Qiu, G.; Cai, Y.; Wang, D.; Li, P.; Shang, L.; Sommar, J. Distribution Patterns of Inorganic Mercury and Methylmercury in Tissues of Rice (*Oryza Sativa L.*) Plants and Possible Bioaccumulation Pathways. *J. Agric. Food Chem.* **2010**, *58*, 4951−4958.

(13) Meng, B.; Feng, X.; Qiu, G.; Liang, P.; Li, P.; Chen, C.; Shang, L. The Process of Methylmercury Accumulation in Rice (*Oryza Sativa L.*). *Environ. Sci. Technol.* **2011**, *45*, 2711−2717.

(14) Aslam, M. W.; Meng, B.; Abdelhafiz, M. A.; Liu, J.; Feng, X. Unravelling the Interactive Effect of Soil and Atmospheric Mercury Influencing Mercury Distribution and Accumulation in the Soil-Rice System. *Sci. Total Environ.* **2022**, *803*, 149967.

(15) Liu, J.; Meng, B.; Poulain, A. J.; Meng, Q.; Feng, X. Stable Isotope Tracers Identify Sources and Transformations of Mercury in Rice (*Oryza Sativa L.*) Growing in a Mercury Mining Area. *Fundam. Res.* **2021**, *1*, 259−268.

(16) Qin, C.; Du, B.; Yin, R.; Meng, B.; Fu, X.; Li, P.; Zhang, L.; Feng, X. Isotopic Fractionation and Source Appointment of Methylmercury and Inorganic Mercury in a Paddy Ecosystem. *Environ. Sci. Technol.* **2020**, *54*, 14334−14342.

(17) Cui, W.; Liu, G.; Bezerra, M.; Lagos, D. A.; Li, Y.; Cai, Y. Occurrence of Methylmercury in Rice-Based Infant Cereals and Estimation of Daily Dietary Intake of Methylmercury for Infants. *J. Agric. Food Chem.* **2017**, *65*, 9569−9578.

(18) Kwon, S. Y.; Selin, N. E.; Giang, A.; Karplus, V. J.; Zhang, D. Present and Future Mercury Concentrations in Chinese Rice: Insights from Modeling. *Global Biogeochem. Cycles* **2018**, *32*, 437−462.

(19) Liu, M.; Zhang, Q.; Cheng, M.; He, Y.; Chen, L.; Zhang, H.; Cao, H.; Shen, H.; Zhang, W.; Tao, S.; Wang, X. Rice Life Cycle-Based Global Mercury Biotransport and Human Methylmercury Exposure. *Nat. Commun.* **2019**, *10*, 5164.

(20) Bravo, A. G.; Cosio, C. Biotic Formation of Methylmercury: A Bio-Physico-Chemical Conundrum. *Limnol. Oceanogr.* **2020**, *65*, 1010−1027.

(21) Li, Y.; Zhao, J.; Zhong, H.; Wang, Y.; Li, H.; Li, Y.-F.; Liem-Nguyen, V.; Jiang, T.; Zhang, Z.; Gao, Y.; et al. Understanding Enhanced Microbial MeHg Production in Mining- Contaminated Paddy Soils under Sulfate Amendment: Changes in Hg Mobility or Microbial Methylators? *Environ. Sci. Technol.* **2019**, *53*, 1844−1852.

(22) Wu, Q.; Hu, H.; Meng, B.; Wang, B.; Poulain, A. J.; Zhang, H.; Liu, J.; Bravo, A. G.; Bishop, K.; Bertilsson, S.; Feng, X. Methanogenesis Is an Important Process in Controlling MeHg Concentration in Rice Paddy Soils Affected by Mining Activities. *Environ. Sci. Technol.* **2020**, *54*, 13517−13526.

(23) Rothenberg, S. E.; Feng, X. Mercury Cycling in a Flooded Rice Paddy. *J. Geophys. Res.: Biogeosci.* **2012**, *117*, 1−16.

(24) Wang, J.; Shaheen, S. M.; Jing, M.; Anderson, C. W. N.; Swertz, A. C.; Wang, S. L.; Feng, X.; Rinklebe, J. Mobilization, Methylation, and Demethylation of Mercury in a Paddy Soil under Systematic Redox Changes. *Environ. Sci. Technol.* **2021**, *55*, 10133−10141.

(25) Liu, J.; Lu, B.; Poulain, A. J.; Zhang, R.; Zhang, T.; Feng, X.; Meng, B. The Underappreciated Role of Natural Organic Matter Bond Hg(II) and Nanoparticulate HgS as Substrates for Methylation in Paddy Soils across a Hg Concentration Gradient. *Environ. Pollut.* **2022**, *292*, 118321.

(26) Liu, J.; Zhao, L.; Kong, K.; Abdelhafiz, M. A.; Tian, S.; Jiang, T.; Meng, B.; Feng, X. Uncovering geochemical fractionation of the newly deposited Hg in paddy soil using a stable isotope tracer. *J. Hazard. Mater.* **2022**, *433*, 128752.

(27) Cui, L.; Feng, X.; Lin, C. J.; Wang, X.; Meng, B.; Wang, X.; Wang, H. Accumulation and Translocation of ^{198}Hg in Four Crop Species. *Environ. Toxicol. Chem.* **2014**, *33*, 334−340.

(28) Strickman, R. J.; Mitchell, C. P. J. Accumulation and Translocation of Methylmercury and Inorganic Mercury in *Oryza*

Sativa: An Enriched Isotope Tracer Study. *Sci. Total Environ.* **2017**, *574*, 1415−1423.
(29) Skyllberg, U.; Persson, A.; Tjerngren, I.; Kronberg, R.; Drott, A.; Meili, M.; Bjorn, E. Chemical Speciation of Mercury, Sulfur and Iron in a Dystrophic Boreal Lake Sediment, as Controlled by the Formation of Mackinawite and Framboidal Pyrite. *Geochim. Cosmochim. Acta* **2021**, *294*, 106−125.
(30) Drott, A.; Björn, E.; Bouchet, S.; Skyllberg, U. Refining Thermodynamic Constants for Mercury(II)-Sulfides in Equilibrium with Metacinnabar at Sub-Micromolar Aqueous Sulfide Concentrations. *Environ. Sci. Technol.* **2013**, *47*, 4197−4203.
(31) Liem-Nguyen, V.; Skyllberg, U.; Nam, K.; Björn, E. Thermodynamic Stability of Mercury(II) Complexes Formed with Environmentally Relevant Low-Molecular-Mass Thiols Studied by Competing Ligand Exchange and Density Functional Theory. *Environ. Chem.* **2017**, *14*, 243−253.
(32) Zhang, T.; Kucharzyk, K. H.; Kim, B.; Deshusses, M. A.; Hsu-Kim, H. Net Methylation of Mercury in Estuarine Sediment Microcosms Amended with Dissolved, Nanoparticulate, and Microparticulate Mercuric Sulfides. *Environ. Sci. Technol.* **2014**, *48*, 9133−9141.
(33) Tian, L.; Guan, W.; Ji, Y.; He, X.; Chen, W.; Alvarez, P. J. J.; Zhang, T. Microbial methylation potential of mercury sulfide particles dictated by surface structure. *Nat. Geosci.* **2021**, *14*, 409−416.
(34) Guo, Y.; Xiang, Y.; Liu, G.; Chen, Y.; Liu, Y.; Song, M.; Li, Y.; Shi, J.; Hu, L.; Yin, Y.; Cai, Y.; Jiang, G. Trojan Horse" Type Internalization Increases the Bioavailability of Mercury Sulfide Nanoparticles and Methylation after Intracellular Dissolution. *ACS Nano* **2023**, *17*, 1925−1934.
(35) Compeau, G. C.; Bartha, R. Sulfate-Reducing Bacteria: Principal Methylators of Mercury in Anoxic Estuarine Sediment. *Appl. Environ. Microbiol.* **1985**, *50*, 498−502.
(36) Gilmour, C. C.; Henry, E. A.; Mitchell, R. Sulfate Stimulation of Mercury Methylation in Freshwater Sediments. *Environ. Sci. Technol.* **1992**, *26*, 2281−2287.
(37) Jeremiason, J. D.; Engstrom, D. R.; Swain, E. B.; Nater, E. A.; Johnson, B. M.; Almendinger, J. E.; Monson, B. A.; Kolka, R. K. Sulfate Addition Increases Methylmercury Production in an Experimental Wetland. *Environ. Sci. Technol.* **2006**, *40*, 3800−3806.
(38) Coleman Wasik, J. K.; Mitchell, C. P. J.; Engstrom, D. R.; Swain, E. B.; Monson, B. A.; Balogh, S. J.; Jeremiason, J. D.; Branfireun, B. A.; Eggert, S. L.; Kolka, R. K.; Almendinger, J. E. Methylmercury Declines in a Boreal Peatland When Experimental Sulfate Deposition Decreases. *Environ. Sci. Technol.* **2012**, *46*, 6663−6671.
(39) Coleman Wasik, J. K.; Engstrom, D. R.; Mitchell, C. P. J.; Swain, E. B.; Monson, B. A.; Balogh, S. J.; Jeremiason, J. D.; Branfireun, B. A.; Kolka, R. K.; Almendinger, J. E. The Effects of Hydrologic Fluctuation and Sulfate Regeneration on Mercury Cycling in an Experimental Peatland. *J. Geophys. Res.: Biogeosci.* **2015**, *120*, 1697−1715.
(40) Hinckley, E. L. S.; Crawford, J. T.; Fakhraei, H.; Driscoll, C. T. A Shift in Sulfur-Cycle Manipulation from Atmospheric Emissions to Agricultural Additions. *Nat. Geosci.* **2020**, *13*, 597−604.
(41) Feinberg, A.; Stenke, A.; Peter, T.; Hinckley, E.-L. S.; Driscoll, C. T.; Winkel, L. H. E. Reductions in the Deposition of Sulfur and Selenium to Agricultural Soils Pose Risk of Future Nutrient Deficiencies. *Commun. Earth Environ.* **2021**, *2*, 101.
(42) National Bureau of Statistics of China. *China Statistical Yearbook*, 2021.
(43) Li, X.; Tyl, C. E.; Kaiser, D. E.; Annor, G. A. Effect of Sulfur Fertilization Rates on Wheat (*Triticum Aestivum L.*) Functionality. *J. Cereal Sci.* **2019**, *87*, 292−300.
(44) Wang, Y.; Wei, Z.; Zeng, Q.; Zhong, H. Amendment of Sulfate with Se into Soils Further Reduces Methylmercury Accumulation in Rice. *J. Soils Sediments* **2016**, *16*, 2720−2727.
(45) Li, Y.; Wang, Y.; Zhang, Q.; Hu, W.; Zhao, J.; Chen, Y.; Zhong, H.; Wang, G.; Zhang, Z.; Gao, Y. Elemental Sulfur Amendment Enhance Methylmercury Accumulation in Rice (*Oryza Sativa L.*) Grown in Hg Mining Polluted Soil. *J. Hazard. Mater.* **2019**, *379*, 120701.
(46) Li, Y.; Lu, C.; Zhu, N.; Chao, J.; Hu, W.; Zhang, Z.; Wang, Y.; Liang, L.; Chen, J.; Xu, D.; Gao, Y.; Zhao, J. Mobilization and Methylation of Mercury with Sulfur Addition in Paddy Soil: Implications for Integrated Water-Sulfur Management in Controlling Hg Accumulation in Rice. *J. Hazard. Mater.* **2022**, *430*, 128447.
(47) Lei, P.; Tang, C.; Wang, Y.; Wu, M.; Kwong, R. W. M.; Jiang, T.; Zhong, H. Understanding the Effects of Sulfur Input on Mercury Methylation in Rice Paddy Soils. *Sci. Total Environ.* **2021**, *778*, 146325.
(48) Yin, D.; He, T.; Yin, R.; Zeng, L. Effects of Soil Properties on Production and Bioaccumulation of Methylmercury in Rice Paddies at a Mercury Mining Area, China. *J. Environ. Sci.* **2018**, *68*, 194−205.
(49) Mao, Y.; Li, Y.; Richards, J.; Cai, Y. Investigating Uptake and Translocation of Mercury Species by Sawgrass (*Cladium Jamaicense*) Using a Stable Isotope Tracer Technique. *Environ. Sci. Technol.* **2013**, *47*, 9678−9684.
(50) Meng, B.; Li, Y.; Cui, W.; Jiang, P.; Liu, G.; Wang, Y.; Richards, J.; Feng, X.; Cai, Y. Tracing the Uptake, Transport, and Fate of Mercury in Sawgrass (*Cladium Jamaicense*) in the Florida Everglades Using a Multi-Isotope Technique. *Environ. Sci. Technol.* **2018**, *52*, 3384−3391.
(51) Qvarnström, J.; Frech, W. Mercury Species Transformations during Sample Pre-Treatment of Biological Tissues Studied by HPLC-ICP-MS. *J. Anal. At. Spectrom.* **2002**, *17*, 1486−1491.
(52) Hintelmann, H.; Keppel-Jones, K.; Evans, D. Constants of mercury methylation and demethylation rates in sediments and comparison of tracer and ambient mercury availability. *Environ. Toxicol. Chem.* **2000**, *19*, 2204−2211.
(53) Jonsson, S.; Skyllberg, U.; Nilsson, M. B.; Westlund, P.; Shchukarev, A.; Lundberg, E.; Bjorn, E. Mercury Methylation Rates for Geochemically Relevant Hg^{II} Species in Sediments. *Environ. Sci. Technol.* **2012**, *46*, 11653−11659.
(54) Olsen, T. A.; Muller, K. A.; Painter, S. L.; Brooks, S. C. Kinetics of Methylmercury Production Revisited. *Environ. Sci. Technol.* **2018**, *52*, 2063−2070.
(55) Landa, E. R. The retention of metallic mercury vapor by soils. *Geochim. Cosmochim. Acta* **1978**, *42*, 1407−1411.
(56) Wang, Y.; Li, Y.; Liu, G.; Wang, D.; Jiang, G.; Cai, Y. Elemental Mercury in Natural Waters: Occurrence and Determination of Particulate Hg(0). *Environ. Sci. Technol.* **2015**, *49*, 9742−9749.
(57) Liu, Y.; Delgado-Baquerizo, M.; Bi, L.; Zhu, J.; He, J. Z. Consistent Responses of Soil Microbial Taxonomic and Functional Attributes to Mercury Pollution across China. *Microbiome* **2018**, *6*, 183−212.
(58) Pu, Q.; Zhang, K.; Poulain, A. J.; Liu, J.; Zhang, R.; Abdelhafiz, M. A.; Meng, B.; Feng, X. Mercury Drives Microbial Community Assembly and Ecosystem Multifunctionality across a Hg Contamination Gradient in Rice Paddies. *J. Hazard. Mater.* **2022**, *435*, 129055.
(59) Bravo, A. G.; Bouchet, S.; Tolu, J.; Björn, E.; Mateos-Rivera, A.; Bertilsson, S. Molecular Composition of Organic Matter Controls Methylmercury Formation in Boreal Lakes. *Nat. Commun.* **2017**, *8*, 14255.
(60) Tuominen, L.; Kairesalo, T.; Hartikainen, H. Comparison of Methods for Inhibiting Bacterial Activity in Sediment. *Appl. Environ. Microbiol.* **1994**, *60*, 3454−3457.
(61) Colombo, M. J.; Ha, J.; Reinfelder, J. R.; Barkay, T.; Yee, N. Oxidation of Hg(0) to Hg(II) by Diverse Anaerobic Bacteria. *Chem. Geol.* **2014**, *363*, 334−340.
(62) Colombo, M. J.; Ha, J.; Reinfelder, J. R.; Barkay, T.; Yee, N. Anaerobic Oxidation of Hg(0) and Methylmercury Formation by *Desulfovibrio Desulfuricans* ND132. *Geochim. Cosmochim. Acta* **2013**, *112*, 166−177.
(63) Hu, H.; Lin, H.; Zheng, W.; Tomanicek, S. J.; Johs, A.; Feng, X.; Elias, D. A.; Liang, L.; Gu, B. Oxidation and Methylation of Dissolved Elemental Mercury by Anaerobic Bacteria. *Nat. Geosci.* **2013**, *6*, 751−754.

https://doi.org/10.1021/acs.est.3c02676
Environ. Sci. Technol. 2023, 57, 8149−8160

(64) Lin, H.; Morrell-Falvey, J. L.; Rao, B.; Liang, L.; Gu, B. Coupled Mercury-Cell Sorption, Reduction, and Oxidation on Methylmercury Production by *Geobacter Sulfurreducens* PCA. *Environ. Sci. Technol.* **2014**, *48*, 11969−11976.
(65) Zheng, W.; Liang, L.; Gu, B. Mercury Reduction and Oxidation by Reduced Natural Organic Matter in Anoxic Environments. *Environ. Sci. Technol.* **2012**, *46*, 292−299.
(66) Poulin, B. A.; Ryan, J. N.; Tate, M. T.; Krabbenhoft, D. P.; Hines, M. E.; Barkay, T.; Schaefer, J.; Aiken, G. R. Geochemical Factors Controlling Dissolved Elemental Mercury and Methylmercury Formation in Alaskan Wetlands of Varying Trophic Status. *Environ. Sci. Technol.* **2019**, *53*, 6203−6213.
(67) Zhang, L.; Wu, S.; Zhao, L.; Lu, X.; Pierce, E. M.; Gu, B. Mercury Sorption and Desorption on Organo-Mineral Particulates as a Source for Microbial Methylation. *Environ. Sci. Technol.* **2019**, *53*, 2426−2433.
(68) Xiang, Y.; Guo, Y.; Liu, G.; Liu, Y.; Song, M.; Shi, J.; Hu, L.; Yin, Y.; Cai, Y.; Jiang, G. Particle-Bound Hg(II) Is Available for Microbial Uptake as Revealed by a Whole-Cell Biosensor. *Environ. Sci. Technol.* **2022**, *56*, 6754−6764.
(69) Grégoire, D. S.; Poulain, A. J. Shining Light on Recent Advances in Microbial Mercury Cycling. *Facets* **2018**, *3*, 858−879.
(70) Lu, X.; Liu, Y.; Johs, A.; Zhao, L.; Wang, T.; Yang, Z.; Lin, H.; Elias, D. A.; Pierce, E. M.; Liang, L.; Barkay, T.; Gu, B. Anaerobic Mercury Methylation and Demethylation by *Geobacter Bemidjiensis Bem*. *Environ. Sci. Technol.* **2016**, *50*, 4366−4373.
(71) Grégoire, D. S.; Lavoie, N. C.; Poulain, A. J. *Heliobacteria* Reveal Fermentation as a Key Pathway for Mercury Reduction in Anoxic Environments. *Environ. Sci. Technol.* **2018**, *52*, 4145−4153.
(72) Shi, L.; Richardson, D. J.; Wang, Z.; Kerisit, S. N.; Rosso, K. M.; Zachara, J. M.; Fredrickson, J. K. The Roles of Outer Membrane Cytochromes of *Shewanella* and *Geobacter* in Extracellular Electron Transfer. *Environ. Microbiol. Rep.* **2009**, *1*, 220−227.
(73) Begley, T. P.; Walts, A. E.; Walsh, C. T. Bacterial organomercurial lyase-overproduction, isolation, and characterization. *Biochemistry* **1986**, *25*, 7186−7192.
(74) Barkay, T.; Gu, B. Demethylation-The Other Side of the Mercury Methylation Coin: A Critical Review. *ACS Environ. Au* **2022**, *2*, 77−97.
(75) Zhou, X.; Hao, Y.; Gu, B.; Feng, J.; Liu, Y.; Huang, Q. Microbial Communities Associated with Methylmercury Degradation in Paddy Soils. *Environ. Sci. Technol.* **2020**, *54*, 7952−7960.
(76) Oremland, R. S.; Culbertson, C. W.; Winfrey, M. R. Methylmercury decomposition in sediments and bacterial cultures? involvement of methanogens and sulfate reducers in oxidative demethylation. *Appl. Environ. Microbiol.* **1991**, *57*, 130−137.
(77) Hsu-Kim, H.; Kucharzyk, K. H.; Zhang, T.; Deshusses, M. A. Mechanisms Regulating Mercury Bioavailability for Methylating Microorganisms in the Aquatic Environment: A Critical Review. *Environ. Sci. Technol.* **2013**, *47*, 2441−2456.
(78) Jørgensen, B. B. The Sulfur Cycle of Freshwater Sediments: Role of Thiosulfate. *Limnol. Oceanogr.* **1990**, *35*, 1329−1342.
(79) Schippers, A. Biogeochemistry of metal sulfide oxidation in mining environments, sediments, and soils. In *Sulfur Biogeochemistry: Past and Present*; Amend, J. P., Edwards, K. J., Lyons, T. W., Eds.; Geological Society of America: Boulder, Colorado, 2004.
(80) Zopfi, J.; Böttcher, M. E.; Jørgensen, B. B. Biogeochemistry of Sulfur and Iron in Thioploca-Colonized Surface Sediments in the Upwelling Area off Central Chile. *Geochim. Cosmochim. Acta* **2008**, *72*, 827−843.
(81) Yuan, D.; Wang, G.; Hu, C.; Zhou, S.; Clough, T. J.; Wrage-Mönnig, N.; Luo, J.; Qin, S. Electron Shuttle Potential of Biochar Promotes Dissimilatory Nitrate Reduction to Ammonium in Paddy Soil. *Soil Biol. Biochem.* **2022**, *172*, 108760.
(82) Todorova, S. G.; Driscoll, C. T.; Matthews, D. A.; Effler, S. W.; Hines, M. E.; Henry, E. A. Evidence for Regulation of Monomethyl Mercury by Nitrate in a Seasonally Stratified, Eutrophic Lake. *Environ. Sci. Technol.* **2009**, *43*, 6572−6578.
(83) Strickman, R. J.; Mitchell, C. P. J. Mercury Methylation in Stormwater Retention Ponds at Different Stages in the Management Lifecycle. *Environ. Sci.: Processes Impacts* **2018**, *20*, 595−606.
(84) Zhang, Y.; Liu, Y. R.; Lei, P.; Wang, Y. J.; Zhong, H. Biochar and Nitrate Reduce Risk of Methylmercury in Soils under Straw Amendment. *Sci. Total Environ.* **2018**, *619−620*, 384−390.
(85) Kögel-knabner, I.; Amelung, W.; Cao, Z.; Fiedler, S.; Frenzel, P.; Jahn, R.; Kalbitz, K.; Kölbl, A.; Schloter, M. Biogeochemistry of Paddy Soils. *Geoderma* **2010**, *157*, 1−14.
(86) Marvin-DiPasquale, M.; Agee, J.; Mcgowan, C.; Oremland, R. S.; Thomas, M.; Krabbenhoft, D.; Gilmour, C. C. Methyl-Mercury Degradation Pathways: A Comparison among Three Mercury-Impacted Ecosystems. *Environ. Sci. Technol.* **2000**, *34*, 4908−4916.
(87) Liu, J.; Liang, J.; Bravo, A. G.; Wei, S.; Yang, C.; Wang, D.; Jiang, T. Anaerobic and Aerobic Biodegradation of Soil-Extracted Dissolved Organic Matter from the Water-Level-Fluctuation Zone of the Three Gorges Reservoir Region, China. *Sci. Total Environ.* **2021**, *764*, 142857.
(88) Orem, W.; Gilmour, C.; Axelrad, D.; Krabbenhoft, D.; Scheidt, D.; Kalla, P.; McCormick, P.; Gabriel, M.; Aiken, G. Sulfur in the South Florida Ecosystem: Distribution, Sources, Biogeochemistry, Impacts, and Management for Restoration. *Crit. Rev. Environ. Sci. Technol.* **2011**, *41*, 249−288.
(89) Santana, M. M.; Dias, T.; Gonzalez, J. M.; Cruz, C. Transformation of Organic and Inorganic Sulfur− Adding Perspectives to New Players in Soil and Rhizosphere. *Soil Biol. Biochem.* **2021**, *160*, 108306.
(90) Wang, J.; Feng, X.; Anderson, C. W. N.; Wang, H.; Wang, L. Thiosulphate-Induced Mercury Accumulation by Plants: Metal Uptake and Transformation of Mercury Fractionation in Soil - Results from a Field Study. *Plant Soil* **2014**, *375*, 21−33.
(91) Wang, J.; Feng, X.; Anderson, C. W. N.; Wang, H.; Zheng, L.; Hu, T. Implications of Mercury Speciation in Thiosulfate Treated Plants. *Environ. Sci. Technol.* **2012**, *46*, 5361−5368.
(92) Vázquez-Rodríguez, A.; Hansel, C. M.; Zhang, T.; Lamborg, C.; Santelli, C. M.; Webb, S.; Brooks, S. Microbial- and Thiosulfate-Mediated Dissolution of Mercury Sulfide Minerals and Transformation to Gaseous Mercury. *Front. Microbiol.* **2015**, *6*, 596.
(93) Liu, T.; Wang, J.; Feng, X.; Zhang, H.; Zhu, Z.; Cheng, S. Spectral Insight into Thiosulfate-Induced Mercury Speciation Transformation in a Historically Polluted Soil. *Sci. Total Environ.* **2019**, *657*, 938−944.
(94) Jørgensen, B. B.; Nelson, D. C. Sulfide Oxidation in Marine Sediments: Geochemistry meets microbiology. *Geol. Soc. Am. Sp. Papers* **2004**, *379*, 63−81.

https://doi.org/10.1021/acs.est.3c02676
Environ. Sci. Technol. 2023, 57, 8149−8160